ORIGINAL RESEARCH ARTICLE

Refinement Mechanism of Primary Carbides in H13 Die Steel Solidified in Super-Gravity Field

SHAOYING LI, XIAOJUN XI, SHUYANG QIN, HANJIE GUO, and JING GUO

In this study, the super-gravity field was used to refine primary carbides in H13 die steel. In the range of super-gravity coefficient of 40 to 140, the influences of super-gravity coefficient on the particle size distribution of primary carbides and the interdendritic element segregation were investigated. The formation time and the maximum generation radius of primary carbides were calculated, and the detailed mechanism of refining primary carbides was discussed. The experimental results show that an increase in the super-gravity coefficient is beneficial to reduce the size and quantity of primary carbides. When the super-gravity coefficient increases from 40 to 140, the quantity of primary carbides in the H13 samples solidified in super-gravity field decreases by 44 pct, and the size of the primary carbides decreases by 15.49 pct. The reason is that increasing the super-gravity coefficient can reduce the degree of interdendrite segregation of elements, and delay the growth time of primary carbides. Compared with VC, the growth time of Mo_2C is more easily affected by the super-gravity coefficient. When the super-gravity coefficient increases from 40 to 140, the solid fraction at which Mo_2C begins to form increases from 0.956 to 0.989.

https://doi.org/10.1007/s11663-022-02597-0

I. INTRODUCTION

H13 die steel with high strength, high hardness, high toughness, and good temper resistance is widely used in extrusion, die casting, hot forging, and other industries.[1,2] To ensure good performance, H13 steel contains a relatively high content of chromium, molybdenum, and vanadium, and higher content of solute elements inevitably leads to dendrite segregation during solidification.[3] Therefore, the coarse primary carbides can be easily generated, resulting to the decrease of the mechanical properties of products.[4,5]

To control the quantity and size of primary carbides, the researchers have done a lot of work,[6–16] including adjusting the composition of H13 steel,[6–9] forging,[10] high-temperature diffusion of the ingot,[11,12] and controlling the parameters of the solidification process.[13–16] Adding appropriate content of rare earth elements or magnesium elements to H13 steel can refine the primary carbides.[6–8] However, when the addition amount of these elements is too large, it will lead to the deterioration of as-cast structure and the decline of material properties.[9] Although forging can break the primary carbides and change its distribution in the matrix, it cannot completely eliminate the primary carbides.[10] High-temperature diffusion can eliminate primary carbides, and the decomposition degree of primary carbides increases with the increase of the high-temperature diffusion temperature.[11,12] However, the higher temperature will cause the crystal grains in the matrix to increase significantly, which limits the application of higher high-temperature diffusion temperature in industrial production. Many researchers believe that the solidification cooling rate has a significant effect on the characteristics of primary carbides.[13,14] Ma *et al.*[15] and Mao *et al.*[16] have clarified that increasing the cooling rate is beneficial to refine the primary carbides. Although increasing the cooling rate can effectively inhibit the coarsening of primary carbides, it is difficult to control the cooling rate inside the large-sized H13 ingots.

Some scholars believe that external interference such as vibration or stirring causes relative movement of the solid and liquid phases in the solidification two-phase zone, which can effectively reduce the segregation of solute elements and control the formation of primary

SHAOYING LI, HANJIE GUO, and JING GUO are with the School of Metallurgical and Ecological Engineering, University of Science and Technology Beijing (USTB), Beijing 100083, P.R. China and also with the Beijing Key Laboratory of Special Melting and Preparation of High-End Metal Materials, Beijing 100083, P.R. China. Contact e-mail: Guohanjie@ustb.edu.cn XIAOJUN XI is with the Beijing Beiye Functional Materials Corporation, Beijing, 100192, China. SHUYANG QIN is with the School of Metallurgical and Ecological Engineering, University of Science and Technology Beijing (USTB).

Manuscript submitted December 8, 2021; accepted July 15, 2022.
Article published online August 10, 2022.

carbides. These external interference methods include electromagnetic stirring technology,[17] mechanical stirring technology,[18] semi-solid casting technology,[19] solidification with pressure,[20] and other new technologies. As an emerging external physical field, the super-gravity technology has the advantages of low use cost and strong operability, which is widely used in many fields such as the recovery of valuable components,[21–26] the removal of inclusions,[27,28] and the refinement of grains.[29,30] For instance, Li *et al.* reported that the enriching perovskite phase could be effectively obtained from $CaO–TiO_2–SiO_2–Al_2O_3–MgO$ melt in a super-gravity field, and the recovery ratio of Ti in the concentrate is up to 74.16 pct.[21] The recovery method is also applied to enriching the TiC from the Cu–Ti–C system,[22] the suanite ($Mg_2B_2O_5$) crystals from boron bearing slag,[23] the Fe-bearing and P-bearing phases from steelmaking slag,[24] the anosovite crystals[25] and the copper phase and iron-rich phase from copper slag,[26] and so on. Song *et al.*[27] studied the separating behavior of non-metallic inclusions in molten aluminum under super-gravity field. Guo *et al.*[28] proposed that the removal of tramp elements within 7075 alloys by super-gravity aided rheorefining method. In addition, Yang *et al.*[29] investigated the refinement mechanism of super-gravity on the solidification structure of Al–Cu alloys, and the results showed that the super-gravity could promote the multiplication of crystal nuclei and strengthen the migration of crystal nuclei within the alloy. Zhao *et al.*[30] also applied the super-gravity to the grain refinement of industrial pure aluminum, and they found that the fragments of dendrite generated by super-gravity could act as the nucleation sites and refine grains.

According to the previous research results,[29,30] it can be found that super-gravity can effectively break the preferentially formed solid phase during solidification. Since the primary carbides of H13 steel are generated in the solidification process, it is speculated that it is feasible to refine the primary carbides in super-gravity field. Therefore, in this work, the super-gravity field is proposed to refine the primary carbides during the solidification of H13 steel. The size distribution of primary carbides and the degree of interdendritic segregation of elements in samples solidified in super-gravity field were investigated, and the generation timing and the maximum generation radius of primary carbides were calculated. Meanwhile, the refinement mechanism of primary carbides in super-gravity field was discussed.

II. MATERIALS AND METHODS

The main element contents of H13 steel were measured by a spark-optical emission spectrometer. The oxygen and nitrogen contents in the metallic phase were analyzed by an oxygen and nitrogen hydrogen analyzer (TCH600, LECO, San Jose, CA). The chemical composition control range of the sample is listed in Table I. The composition of the molten slag is listed in Table II.

The super-gravity equipment used in the study was self-refitted by a J55 series vertical centrifuge produced by a company in Gansu, China. The device is mainly composed of a solidification mold and a centrifugal system, which has a rated power of 18 KW and a maximum speed of 1050 r/min. The super-gravity experiment was performed at room temperature (25 °C), and the experimental process is shown in Figures 1(a) and (b). The molten metal (42 kg) and slag (8 kg) were poured into a rotating mold with a certain rotational speed. Before pouring, the temperature of the mixture of molten steel and slag was 1650 °C ± 20 °C, which was measured by an infrared thermometer (IR-HOH, Beijing Duhelichuang Technology Co. Ltd, Beijing, China). The mixtures of steel and slag were completely poured into the mold within 10 seconds. Due to the density difference between molten slag and molten steel, the small amount of molten slag prior to the molten steel entered into the mold, and the molten slag that entered first quickly formed a slag skin to prevent adhesion of the casting and the mold. Then, the mixture of molten slag and steel entered into the mold, and the centrifugal speed of molten steel was greater than that of slag under the action of super-gravity, which caused that the molten slag easily accumulates to the center of rotation. Finally, the remaining slag liquid was poured into the mold. Since the temperature of the molten slag was higher than that of the molten steel, a solidification field with high center temperature and low edge temperature was formed in the mold. Therefore, the shrinkage cavity in the casting could be supplemented in time to ensure the compactness of the casting. For the samples under super-gravity fields, the cooling rate for all the samples was calculated to approximately 3 °C/s.

To facilitate the study of primary carbides in H13 die steel solidified in super-gravity field, the inner side of the casting is selected as the analysis position, as shown in Figure 1(c). In the study, samples A, B, and C were solidified with the conditions of different super-gravity coefficients, respectively. The super-gravity coefficients of samples A, B, and C were set to 40, 90, and 140, respectively. The super-gravity coefficient is controlled by the rotational speed of the centrifuge. The definition of the super-gravity coefficient[22,23] is given in Eq. [1].

$$G = \frac{\sqrt{g^2 + (\omega^2 R)^2}}{g} = \frac{\sqrt{g^2 + \left(\frac{N^2\pi^2 R}{900}\right)^2}}{g}, \qquad [1]$$

where G is the gravity coefficient, ω is the angular speed (rad/s), N is the rotational speed (r/min), R is the distance between the center of rotation and the observation position (*i.e.*, rotational radius, m), and g is the normal gravitational acceleration (9.8 m/s^2). According to Eq. [1], the rotational speed of samples A, B, and C solidified in super-gravity field were set to 500, 750, and 950 r/min, respectively.

Geminisem 500 field emission scanning electron microscope was used to observe the morphology of primary carbides. ZEISS EVO18 scanning electron microscope (SEM) equipped with ASPEX system was used to analyze the size, composition, and number of the

Table I. Chemical Composition Control Range of the H13 Die Steel (Wt. Pct)

C	Si	Mn	Cr	Mo	V	O	N	Fe
0.46–0.51	0.8–0.9	0.3	4.5–4.6	1.2–1.4	0.9–1.0	≤ 0.004	≤ 0.012	bal.

Table II. Chemical Composition of the Molten Slag (Wt. Pct)

CaO	MgO	CaF_2	Al_2O_3	SiO_2
8.2	18.3	61.3	8.2	4.0

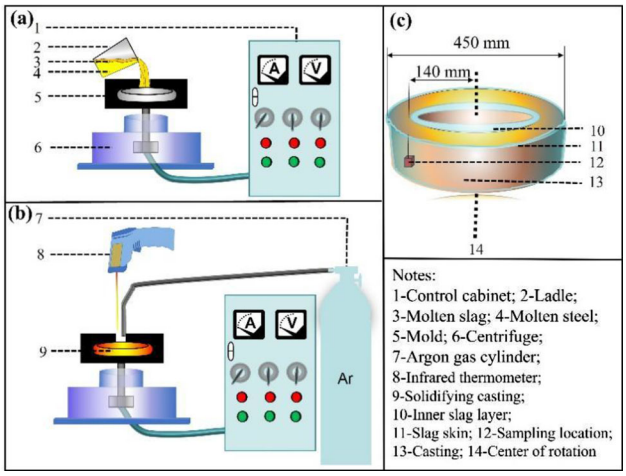

Fig. 1—Schematic diagram of super-gravity solidification experiment process (*a*) Molten steel and slag are poured into the mold; (*b*) The super-gravity casting is solidifying; (*c*) The solidified super-gravity casting.

primary carbides in a square region with dimensions of 4×4 mm^2 in the samples. JSM-7800F field emission scanning electron microscope (FE-SEM) and JXA-8530F field emission electron microprobe analyzer (EPMA) were used to analyze the elements distribution in the samples.

III. RESULTS AND DISCUSSION

A. *Particle Size Distribution of Primary Carbides in Super-Gravity Samples*

According to the composition classification, the primary carbides in H13 die steel can be divided into V-rich primary carbides (abbreviated as V-rich carbides) and Mo-Cr-rich primary carbides (abbreviated as Mo-rich carbides), and there are a small amount of Ti and N elements in some V-rich primary carbides.[16] The typical morphology of primary carbides in H13 castings solidified in super-gravity field is shown in Figure 2. Figure 2(a) shows the V-rich carbides, with a vanadium content of about 41.76 wt. pct; Figure 2(b) shows the composite of V-rich carbides and Mo-rich carbides, and the contents of Mo and Cr in the Mo-rich carbides are about 37.26 and 21.62 wt. pct, respectively; Figure 2(c) shows the magnesium–aluminum spinel (MgO Al_2O_3) and Ti–N-rich V-type primary carbides. Both MgO and Al_2O_3 are produced in the liquid phase, and the V-rich carbides are produced at the solidification front when the solid-phase ratio reaches 0.95,[16] which leads to the formation of V-rich carbides with magnesium–aluminum spinel as the core. In this study, unless otherwise specified, the V-rich carbides with magnesium–aluminum spinel as the core are classified as V-rich carbides.

In samples A, B, and C, Mo-rich carbides, V-rich carbides, and V-rich carbides with Ti and N were randomly selected, and the number of each carbide was twenty. The composition of primary carbides was analyzed by energy spectrometer, and the average composition of various types of primary carbides was statistically analyzed, the results are shown in Figure 3. According to Figure 3, it can be observed that the Mo content in the Mo-rich carbides is about 39 to 42 wt. pct, and the Mo content in the other two types of primary carbides is about 17 to 22 wt. pct; the contents of V element in V-rich carbides, V-rich carbides with Ti and N, and Mo-rich carbides are about 36 to 44 wt. pct, 21 to 25 wt. pct, and 8 to 13 wt. pct, respectively. In order to facilitate the classification, the V-rich carbides with Ti and N are also classified as V-rich carbides.

According to the average composition of primary carbides shown in Figure 3, the types of primary carbides in super-gravity H13 castings are distinguished. The primary carbides with V content greater than 20 wt. pct are classified as V-rich carbides, and the primary carbides with V content less than 20 wt. pct are classified as Mo-rich carbides. The statistical results of the number of primary carbides are shown in Figure 3(b). The super-gravity coefficient corresponding to samples A, B, and C are 40, 90 and 140, respectively. The results show that with the increase of the super-gravity coefficient from 40 to 140, the total number of primary carbides and the number of V-rich primary carbides are significantly reduced, from 1673 and 935 to 1425 and 723, respectively. The number of Mo-rich primary carbides is slightly reduced. It can be inferred from the statistical results that the increase of the super-gravity coefficient is beneficial to reduce the number of primary carbides.

The distribution of the number of primary carbides with different lengths in the samples A, B, and C is shown in Figure 4. Figures 4(a) and (b) show the number and proportion of V-rich primary carbides in different length ranges, respectively. It can be observed

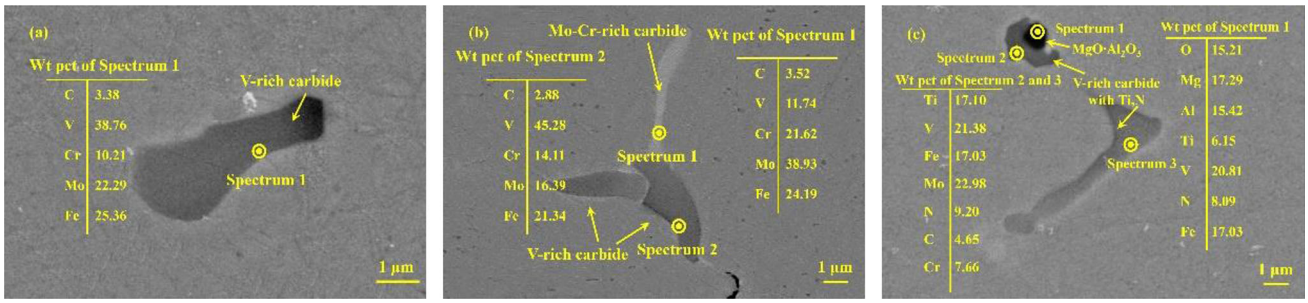

Fig. 2—The morphology and type of primary carbides in samples (*a*) V-rich primary carbides, (*b*) V-rich primary carbides and Mo-Cr-rich primary carbides, (*c*) magnesium–aluminum spinel and V-rich primary carbides with TiN.

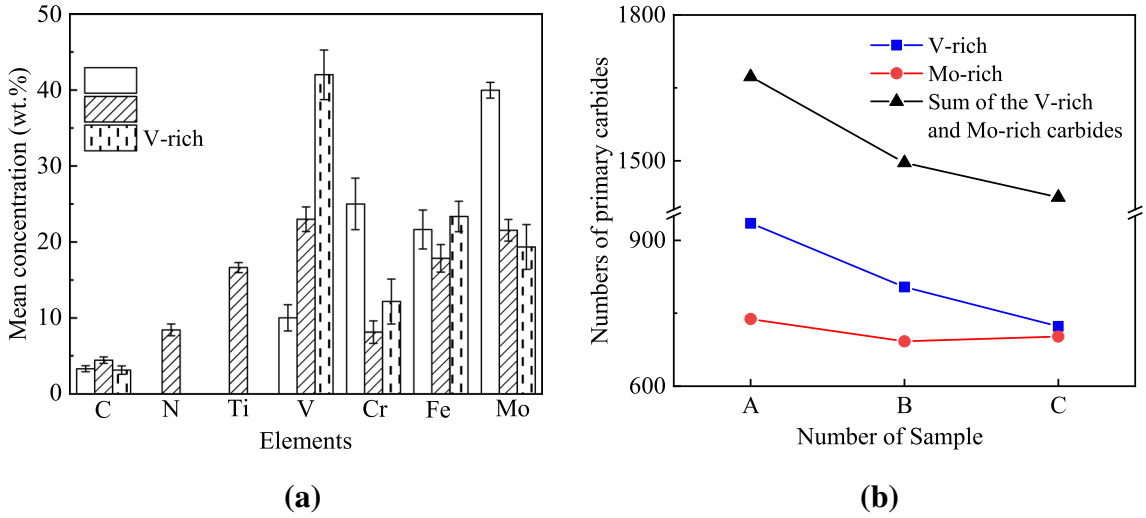

Fig. 3—The elements mean concentration (*a*) and (*b*) numbers of different primary carbides in samples.

from Figures 4(a) and (b) that in the samples A, B, and C, the number of V-rich primary carbides with lengths ranging from 2 to 5 μm and 5 to 10 μm decreases successively. The proportion of V-rich primary carbide with length greater than 5 μm in samples A, B, and C is about 35, 30, and 30 pct, respectively, and the proportion of V-rich primary carbides with length less than 5 μm in A, B, and C is about 65, 70, and 70 pct, respectively. It shows that with the increase of super-gravity coefficient, the number and size of V-rich primary carbides decrease. Figures 4(c) and (d) show the number and proportion of Mo-rich primary carbides in different length ranges, respectively. It can be observed that in samples A, B, and C, Mo-rich primary carbides with a length of less than 5 μm account for 92, 94, and 94 pct, respectively. The number of Mo-rich primary carbides with a length greater than 5 μm in sample A is 58, accounting for about 8 pct. In samples B and C, the number of Mo-rich primary carbides with a length greater than 5 μm are, respectively, 36 and 35, both accounting for about 6 pct. The above results show that with an increase of the super-gravity coefficient from 40 to 90, the number and size of Mo-rich primary carbides decrease, and with an increase of the super-gravity coefficient from 90 to 140, the number and size of Mo-rich primary carbides remained almost unchanged.

The total area and average area of the primary carbides in samples A, B, and C are shown in Figure 5. It can be observed from the figure that as the super-gravity coefficient increases, the total area of primary carbides is significantly reduced from 8843.24 to 6365.48 μm^2, a decrease of 28.0 pct. Among them, the area occupied by the V-rich primary carbides decreases from 6025.24 to 4393.32 μm^2, a decrease of 27.1 pct. The area occupied by the Mo-rich primary carbides decreased from 2818.99 to 1972.16 μm^2, a decrease of 30.0 pct. In addition, with the increase of super-gravity coefficient from 40 to 140, the average area of the primary carbides is reduced by 15.49 pct. Compared with the Mo-rich primary carbides, the average area of the V-rich primary carbide is less affected by the super-gravity coefficient.

Based on the above analysis results, it can be observed that within the super-gravity coefficient range of this study, the number of primary carbides in the H13 steel decreases with the increase of the super-gravity

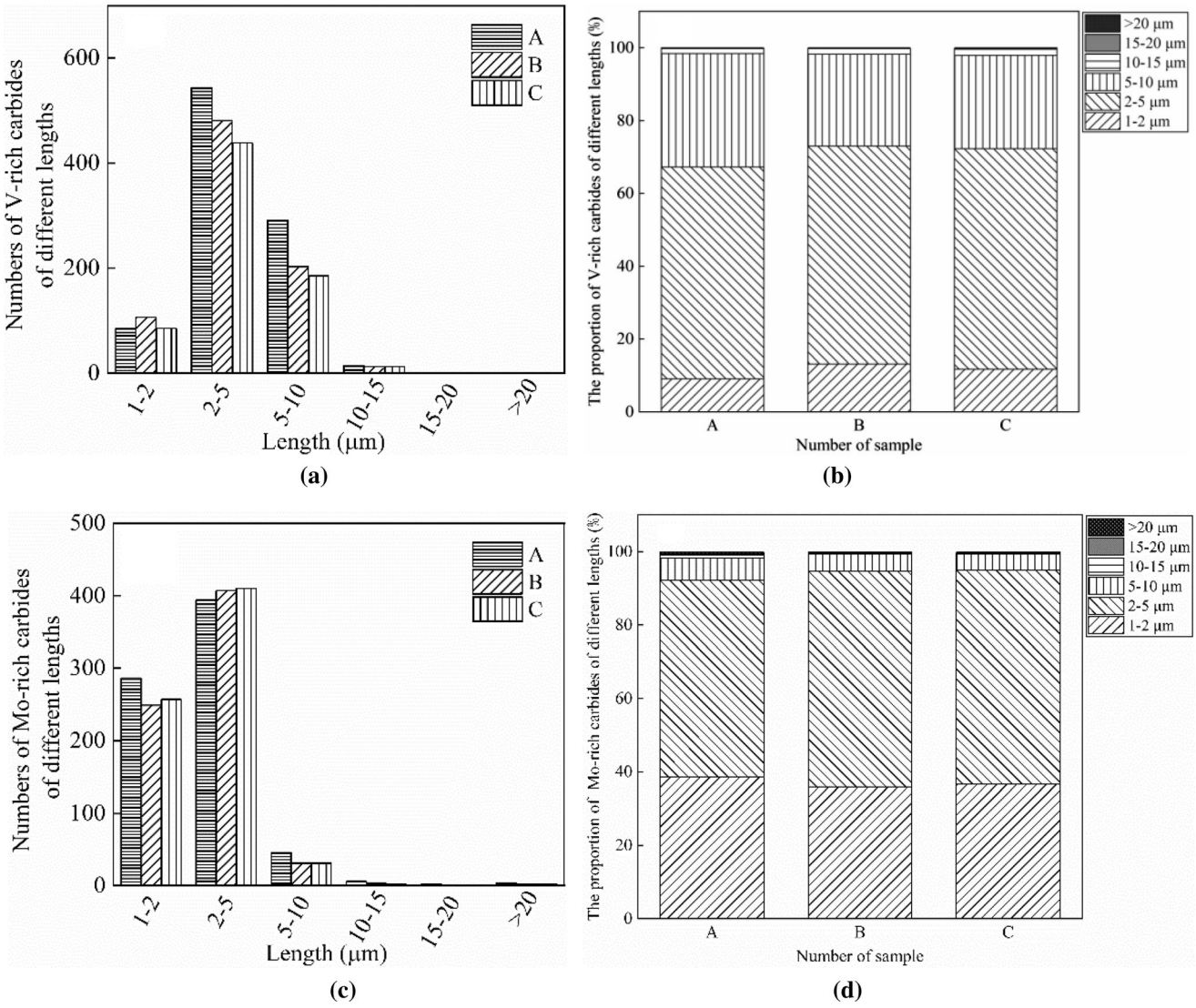

Fig. 4—The size distribution of the primary carbides in samples solidified in the different super-gravity fields (*a*) the number of V-rich carbides with different lengths, (*b*) the proportion of V-rich carbides with different lengths, (*c*) the number of Mo-rich carbides with different lengths, (*d*) the proportion of Mo-rich carbides with different lengths.

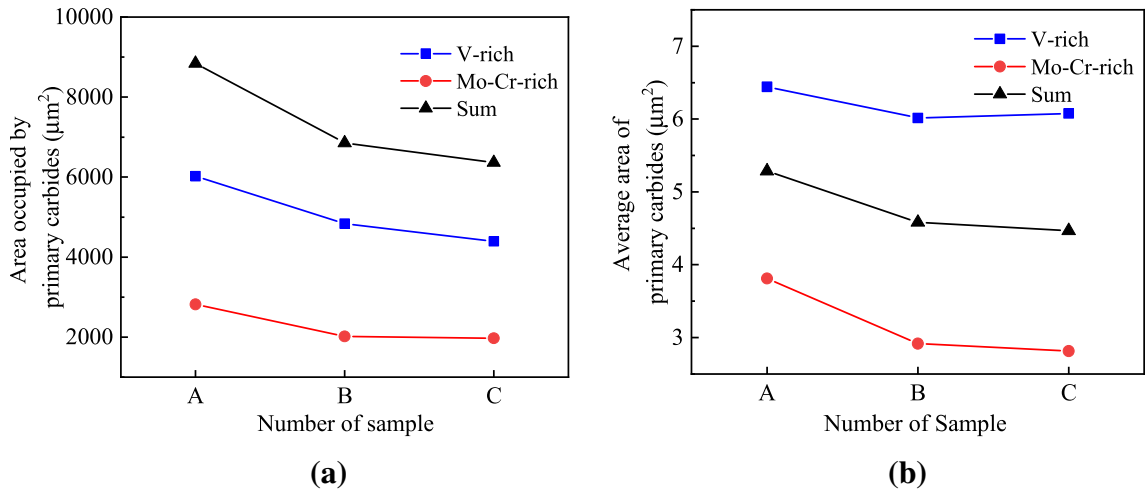

Fig. 5—The area of different primary carbides in different samples (*a*) total area, (*b*) average area.

coefficient; the H13 steel mainly contains V-rich primary carbides with a length of less than 10 μm, and Mo-rich primary carbides with a length of less than 5 μm. In addition, with the increase of the super-gravity coefficients, the number and average size of the Mo-rich and V-rich primary carbides decreased, but the decreasing trend of the average size of V-rich primary carbides is not very obvious.

B. *The Formation and Growth of Primary Carbides in Different Super-Gravity Fields*

Figure 6(a) is the equilibrium phase assemblage diagram of H13 steel during solidification. It can be found that carbides begin to appear in the solid phase during equilibrium solidification. However, the actual solidification process of H13 steel is non-equilibrium. In Figure 6(b), carbides of M_7C_3, M_2C, and MC are formed in the solid–liquid two-phase region with a solid phase ratio greater than 0.9, as shown by the yellow line. The reason is that the content of alloy elements in H13 castings is high, and the alloy elements are prone to segregation in the process of non-equilibrium solidification. Therefore, the segregation degree of alloy elements between dendrites directly affects the growth time and growth size of primary carbides.

1. *Interdendritic element segregation under super-gravity field*

The central positions of the samples A, B, and C are scanned by electron microprobe, and the distribution of C, V, Cr, and Mo elements among the dendrites of the castings solidified in different super-gravity fields were analyzed. The analysis results are shown in Figure 7. In Figure 7, the dark area is the concentration of an element in the dendrite stem, and the light area is the enrichment area of an element between dendrites. The width of the interdendritic element enrichment zone (abbreviated as EEZW) is shown in Figure 7(a), in which the black arrow points to the typical interdendritic primary carbides. It can be observed from Figure 7 that the concentration of an element between dendrites is greater than that of an element in dendrite stem, indicating that the solute element is easy to be enriched between the dendrites. In the same casting, the width of Mo element enrichment zone between dendrites is larger than that of C, V, and Cr elements. When analyzing the same element, compared with castings A and B, the width of interdendritic element enrichment zone in sample C is smaller.

In order to further clarify the influence of super-gravity coefficient on the width of interdendritic element enrichment zone, 10 positions are randomly selected in Figures 7(a) to (l). And the width of interdendritic element enrichment zone of C, V, Cr, and Mo in different castings is counted by Image-pro image analysis software, and the statistical results are shown in Figure 8(a). As can be observed from Figure 8(a), the width of element enrichment zone decreases with the increase of super-gravity coefficient. The reason may be that an increase in the super-gravity coefficient enhances the stirring effect of the super-gravity on the molten steel and increases the destructive ability of the dendrite, which makes the liquid phase with high solute element concentration to fully flow during the solidification process, thus reducing the width of the solute element enrichment zone in the liquid phase.

The concentrations of C, V, Cr, and Mo elements in five interdendritic element enrichment zones and adjacent dendrite stems were collected in the samples A, B, and C, and the measured segregation ratios of four elements were counted. The measured segregation ratio (SR) can be calculated by Eq. [2].

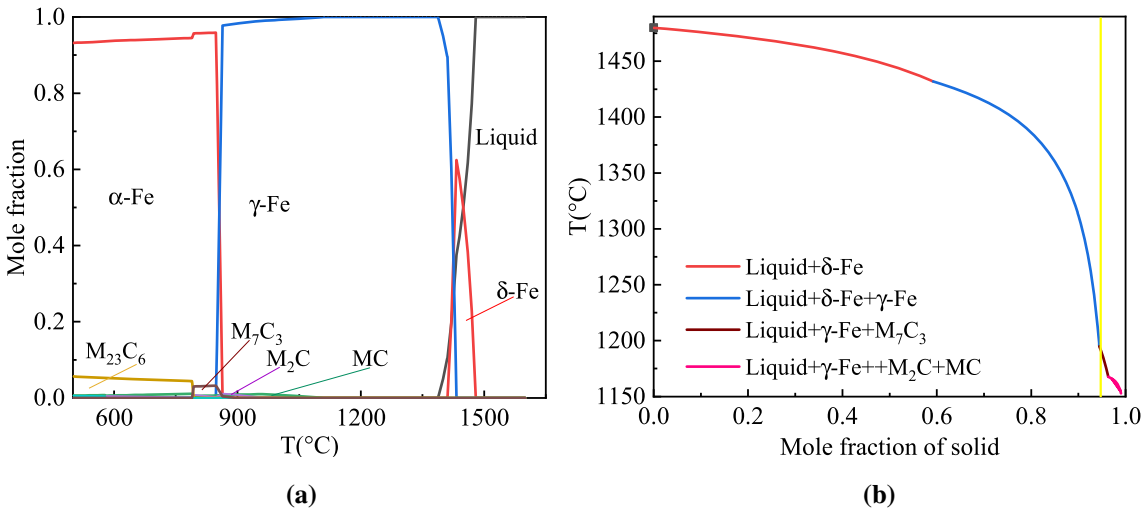

Fig. 6—The phase assemblage diagram of H13 steel calculated by Thermo-Calc (*a*) mole fraction of different equilibrium phases, (*b*) mole fraction of non-equilibrium phase (Notes: δ-Fe is high-temperature ferrite; γ-Fe is austenite; α-Fe is ferrite; $M_{23}C_6$, M_7C_3, M_2C, and MC are carbide types).

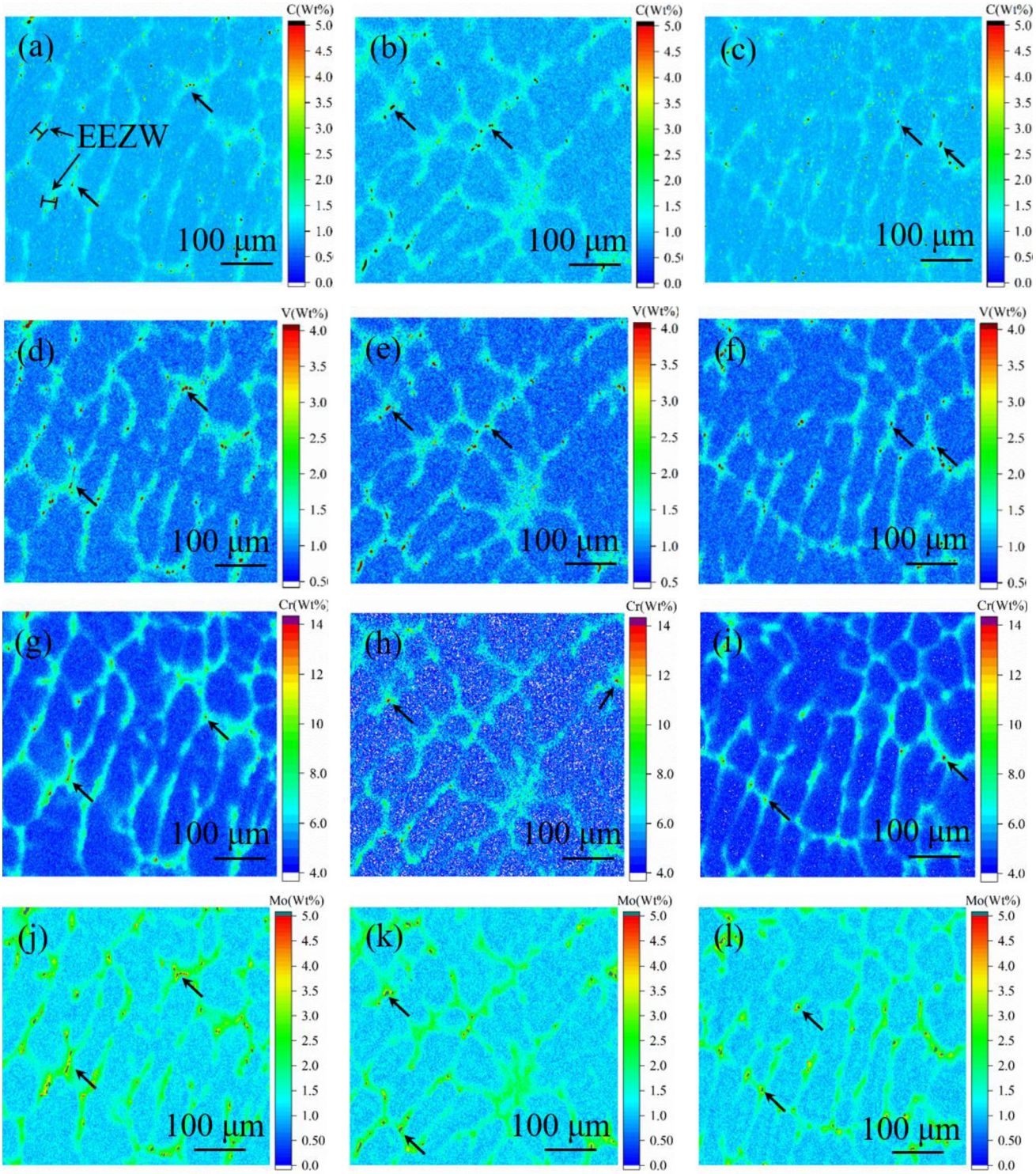

Fig. 7—The concentration distribution of each element in Sample A, Sample B, and Sample C (*a*) C element in Sample A; (*b*) C element in Sample B; (*c*) C element in Sample C; (*d*) V element in Sample A; (*e*) V element in Sample B; (*f*) V element in Sample C; (*g*) Cr element in Sample A (*h*) Cr element in Sample B; (*i*) Cr element in Sample C; (*j*) Mo element in Sample A (*k*) Mo element in Sample B; (*l*) Mo element in Sample C. *Note* EEZW represents the width of the element enrichment zone.

$$SR = \frac{c_{\max}}{c_{\min}}, \qquad [2]$$

where $c_{\max}$ is the maximum concentration of an element between dendrites; $c_{\min}$ is the minimum concentration of an element in the dendrite stem adjacent to the dendrite.

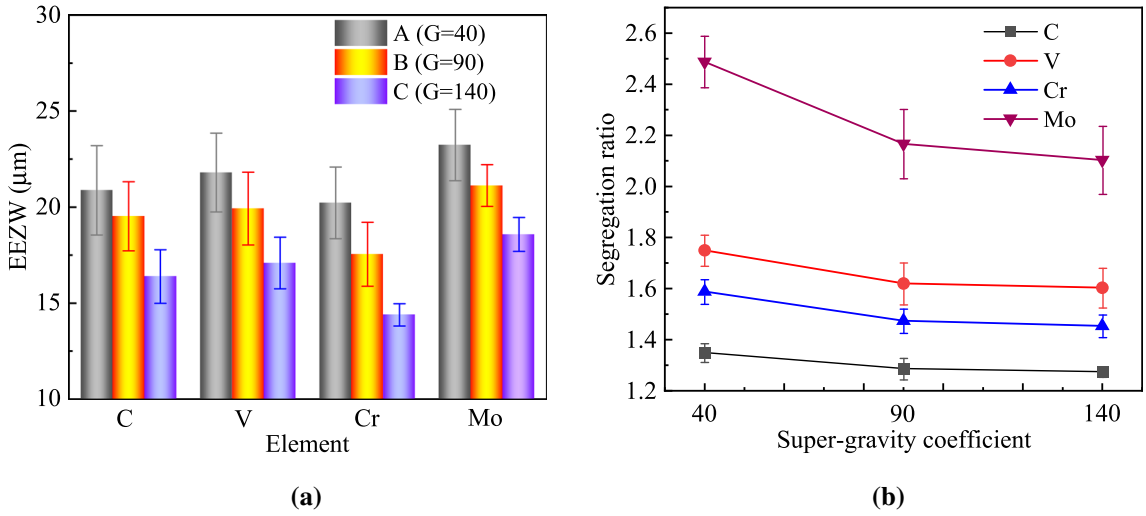

Fig. 8—(*a*) EEZW and (*b*) Element segregation ratio in samples solidified in different super-gravity fields.

The relationship between the segregation ratio of C, V, Cr, and Mo elements and the super-gravity coefficient is shown in Figure 8(b). It can be observed that the segregation ratios of the four elements are all greater than 1, of which the segregation ratio of Mo element is the largest, followed by V, Cr, and C. The segregation ratios of the four elements all decrease with the increase of the super-gravity coefficient, but the segregation ratios of different elements are affected by the super-gravity coefficient to different degrees. Among them, the segregation ratio of Mo is the most affected by the super-gravity coefficient, while the segregation ratio of C is the least affected by the super-gravity coefficient. In addition, an increase of the super-gravity coefficient reduces the element segregation degree. The reason is that increasing the super-gravity coefficient enhances the forced convection of melt caused by super-gravity, which speeds up the movement speed of enriched elements in the solidification front, thus promoting the uniformity of solute elements in the melt.

2. *The growth time of primary carbides under super-gravity field*

According to the analysis results of element segregation between dendrites in different super-gravity field solidified castings, it can be found that the change of the super-gravity coefficient will cause changes in the concentration of certain elements in the solidification front, thus changing the formation time of primary carbides. The distribution of C, V, Cr, and Mo elements in Figure 7 is analyzed by F–G sorting method,[30] and the surface scanning data of the four elements are arranged in ascending order, in which the smallest numerical point is taken as the solidification starting point, namely, the solid fraction is 0; the maximum numerical point is the termination point, that is, the solid fraction is 1. The composition curve is drawn with the solid fraction as the abscissa and the element concentration as the ordinate, and the relationship between element concentration and solid fraction with different super-gravity coefficients is shown in Figure 9.

As can be observed from Figure 9, the element concentration increases with the increase of solid fraction. When the solid fraction is less than 0.8, the element concentration changes little with the increase of solid fraction; when the solid fraction is between 0.8 and 1.0, the element concentration increases linearly with the increase of the solid fraction. Here, the solid fraction when the element concentration begins to show a linear upward trend is called "inflection point." It can be observed from Figure 9(a) that the C element concentration increases with the increase of the solid fraction, when the solid fraction is close to 1, the C element concentration reaches its maximum value; the super-gravity coefficient has little effect on the maximum concentration of C element, but the super-gravity coefficient has a certain effect on the "inflection point," which moves to the right with the increase of super-gravity coefficient. Compared with C element, the super-gravity coefficient has a greater influence on the maximum concentration of V element. When the super-gravity coefficients are 40, 90, and 140, the corresponding maximum concentrations of element V are 27, 20, and 18 wt. pct, respectively, and the corresponding "inflection point" values are 0.92, 0.94, and 0.96, respectively, as shown in Figure 9(b). The super-gravity coefficient has a great influence on the Cr concentration at the initial and end stages of solidification, as shown in Figure 9(c). When the super-gravity coefficient is 40 and the solid fraction is 0 and 1, the Cr concentration is 2.0 and 18.0 wt. pct, respectively. Compared with the Cr concentration distribution at the super-gravity coefficient of 40, the Cr concentration at the super-gravity coefficient of 140 is higher at the initial stage of solidification, with a value of 3.8 wt. pct, and lower at the end stage of solidification, with a value of 9.2 wt. pct. In addition, with the increase of super-gravity coefficient, the "inflection point" does not move to the right obviously. The segregation degree of Mo element is most affected by the super-gravity coefficient, as shown in Figure 9(d). Due to the low content of Mo element in steel, the effect of super-gravity coefficient on

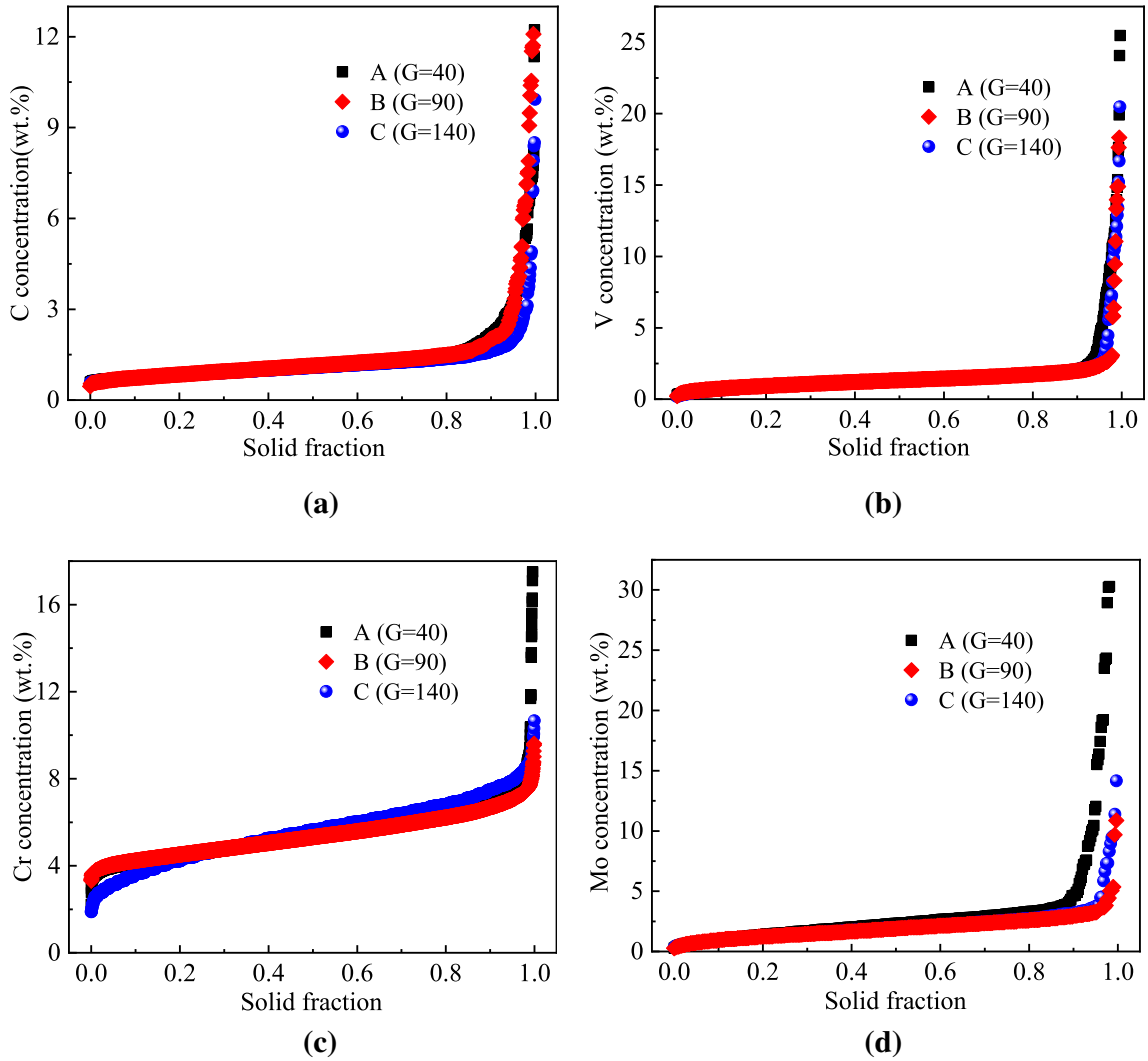

Fig. 9—The relationship between element concentration and solid fraction (*a*) C, (*b*) V, (*c*)Cr, (*d*) Mo.

Mo concentration is not obvious at the initial stage of solidification. At the end stage of solidification, when the super-gravity coefficient is 40, the Mo concentration is 30.5 wt. pct, and the "inflection point" value is 0.91, while when the super-gravity coefficient is 90 and 140, the Mo concentration is 11.4 and 14.6 wt. pct, respectively, and the corresponding "inflection point" values are 0.96 and 0.97, respectively. In summary, increasing the super-gravity coefficient is beneficial to reduce the element segregation degree.

According to the relationship between element concentration and solid fraction under different super-gravity coefficients, combined with the standard Gibbs free energy of various types of carbides, the relationship between the formation reaction of Gibbs free energy of various types of carbides and solid fraction under different super-gravity coefficients can be calculated, thus predicting the formation time of various types of carbides. The formation reaction of carbides in steel can be expressed by Eq. [3].

$$x[M] + y[C] = M_x C_{y(s)}. \quad [3]$$

The reaction Gibbs free energy ΔG can be expressed as

$$\Delta G = \Delta G^{\emptyset} + RT \ln\left(\frac{1}{(f_M[\text{pct } M])^x (f_C[\text{pct } C])^y}\right) \quad [4]$$

$$\log f_i = \sum_{j=2}^{n} e_i^j([\text{pct } j]), \quad [5]$$

where $\Delta G^{\emptyset}$ is the reaction standard Gibbs free energy, kJ mol^{-1}; R is the ideal gas constant with a value of 8.314 J mol^{-1} K^{-1}; T is the reaction temperature, K; f_i is the activity coefficient of the element; e_i^j is the activity interaction coefficient of element j to element i.

In order to simplify the calculation, the precipitated V-rich MC and Mo-rich M_2C were assumed to be VC and Mo_2C, respectively.[16] The standard Gibbs free energy of formation of each carbide is shown in Eqs. [6] and [7].

$$[V] + [C] = VC_{(s)} \quad \Delta G^{\emptyset} = -103990 + 78.28T \quad [6]$$

$$2[\mathrm{Mo}] + [\mathrm{C}] = Mo_2C_{(s)} \quad \Delta G^{\emptyset} = -123410 + 142.84T \qquad [7]$$

When the Gibbs free energy of formation of carbides is less than zero, carbides will be formed in the liquid phase. The primary interaction coefficient between alloy elements used in the calculated process is shown in Table III.[32]

The variation of reaction Gibbs free energy of two types of carbides with solid fraction under different super-gravity coefficients is shown in Figure 10. The reaction Gibbs free energy of carbide at the solidification front decreases with the increase of solid fraction, and when the solid fraction is close to 1, the reaction Gibbs free energy increases greatly with the change of solid fraction. When ΔG is less than 0, carbides can be formed. However, the growth time of different types of carbides is different in the different super-gravity fields.

As shown in Figure 10(a), when the solid fraction is greater than 0.8, the Gibbs free energy generated by the reaction of VC is less than 0, and the super-gravity coefficient has little effect on the Gibbs free energy generated by the reaction, which indicates that increasing the super-gravity coefficient has little effect on the growth time of VC. The super-gravity coefficient affects the growth time of Mo_2C, as shown in Figure 10(b). In the super-gravity field with the super-gravity coefficient of 40, Mo_2C begins to generate when the solid fraction is 0.956; while in the super-gravity field with the super-gravity coefficient of 90 and 140, Mo_2C begins to generate when the solid fraction is 0.989. In summary, in addition to VC, an increase in the super-gravity coefficient is beneficial to delay the growth time of primary carbides in H13 castings.

3. *The maximum generation radius of primary carbides under super-gravity field*

According to the relationship between alloy element concentration and solid fraction in the solidification process of different super-gravity fields, the growth dynamic model of primary carbide is established, so as to clarify the influence of the super-gravity coefficient on the growth of primary carbides. In the solidification process, the factors controlling the growth of primary carbides include the interfacial chemical reaction rate between carbide particles and liquid phase, the mass transfer rate of metal atoms in carbide from liquid phase to reaction interface, and the mass transfer rate of carbon atoms from liquid phase to reaction interface. Generally, the interface reaction is very rapid at high temperature, and the reaction time can be ignored. In addition, according to the diffusion coefficient of carbon atoms and other metal atoms in the liquid phase,[16] the mass transfer rate of carbon atoms from the liquid phase to the reaction interface is much higher than that of other metal atoms. Therefore, the limiting link of primary carbide growth is the mass transfer of metal atoms from the liquid phase to the reaction interface.

In the residual liquid phase at the solidification front, the concentration difference between the metal element concentration and its equilibrium concentration is the driving force for the growth of primary carbides, in which the equilibrium concentration is the metal element concentration corresponding to the reaction Gibbs free energy of carbide to zero. Taking VC as an example, in the solidification process, the diffusion flow density J_V of V mass transfer from the liquid phase at the solidification front to the VC surface can be expressed by Eq. [8].[33]

$$J_V = \frac{D_V^L \rho_{\mathrm{Fe}}}{100 M_V r}\left([\mathrm{pct}\ V]_L - [\mathrm{pct}\ V]_{\mathrm{equilibrium}}\right) \qquad [8]$$

All the V atoms diffused from the liquid phase to the interface of VC particles form VC, which makes the VC particles grow up. Therefore, the relation between VC particle radius and J_V is as follows:

$$4\pi r^2 \mathrm{M_{VC}} J_V \Delta t = \frac{4}{3}\pi \rho_{\mathrm{VC}}\left[(r+\Delta r)^3 - r^3\right]. \qquad [9]$$

The relationship between the radius of VC particles and their growth time can be obtained by simultaneous Eqs. [8] and [9], as shown in Eq. [10].

$$r\frac{\mathrm{d}r}{\mathrm{d}t} = \frac{M_{VC}\rho_{\mathrm{Fe}}}{100 M_V \rho_{VC}} D_V^L\left([\mathrm{pct}\ V]_L - [\mathrm{pct}\ V]_{\mathrm{equilibrium}}\right) \qquad [10]$$

By integrating Eq. [11], the dimensional change of VC during the solidification process can be obtained, which is expressed by the following equations:

$$r_{\mathrm{VC}} = \sqrt{\frac{M_{\mathrm{VC}}\rho_{\mathrm{Fe}}}{50 M_{\mathrm{Fe}}\rho_{\mathrm{VC}}} D_{\mathrm{V}}^{\mathrm{L}}\left([\mathrm{pct}\ V]_{\mathrm{L}} - [\mathrm{pct}\ V]_{\mathrm{equilibrium}}\right) t_{VC}} \qquad [11]$$

$$t_{\mathrm{VC}} = \left[1 - f_{\mathrm{S},VC}\right] t_f \qquad [12]$$

Since the growth time of VC is prior to Mo_2C, VC consumes a large amount of carbon in the generation process. Here, it is considered that the reaction rate is controlled by the mass transfer of C element from liquid phase to the surface of Mo_2C particle. Therefore, the size change of Mo_2C in the solidification process of super-gravity field can be obtained, as shown in Eqs. [13] and [14].

$$r_{\mathrm{Mo_2C}} = \sqrt{\frac{\mathrm{M_{Mo_2C}}\rho_{\mathrm{Fe}}}{50 \mathrm{M_C}\rho_{\mathrm{Mo_2C}}} D_{\mathrm{C}}^{\mathrm{L}}\left([\mathrm{pct\,C}]_{\mathrm{L}} - [\mathrm{pct\,C}]_{\mathrm{equilibrium}}\right) t_{\mathrm{Mo_2C}}} \qquad [13]$$

$$t_{\mathrm{Mo_2C}} = \left[1 - f_{\mathrm{S},Mo_2C}\right] t_f, \qquad [14]$$

Table III. Primary Interaction Coefficient Between Alloy Elements[32]

e_i^j	C	Si	Mn	P	S	Mo	V	Cr	N	Ti
C	0.14	0.08	− 0.012	0.051	0.046	− 0.0083	− 0.038	− 0.024	0.11	− 0.08
Mo	− 0.097	—	0.048	− 0.0066	− 0.0006	0.0121	—	− 0.0003	− 0.1	—
V	− 0.17	0.042	0.0057	-0.041	− 0.028	—	0.015	0.012	− 0.35	—

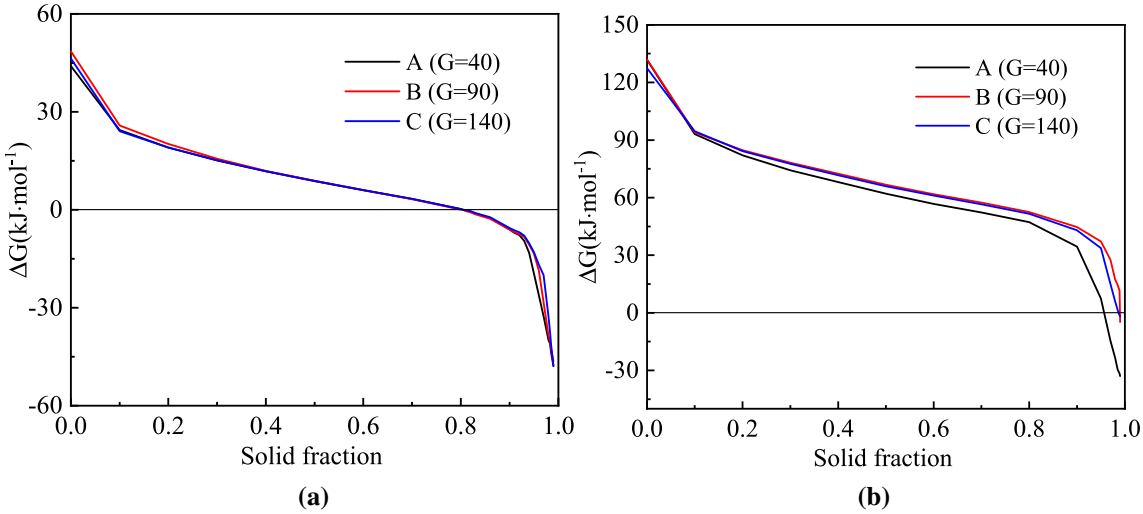

Fig. 10—The relationship between ΔG of carbides with different types and solid fraction (*a*) VC, (*b*) Mo_2C.

where r_{XC} is the maximum generation radius of the carbide particles, m; M_{VC}, M_{Mo_2C} , and M_C are the molar mass of VC, Mo_2C, and C, respectively, g/mol; ρ_{VC}, ρ_{Mo_2C} , and ρ_{Fe} are the density of VC, Mo_2C, and molten steel, respectively, kg/m^3; D_V^L, D_C^L , and D_{Mo}^L are the diffusion coefficients of V, C, and Mo in liquid steel, and the values are 4×10^{-9}, 12×10^{-9}, and 3.8×10^{-9} m^2/s, respectively; [pct V]$_L$ is the mass fraction of V in liquid phase under different super-gravity fields, and its value can be obtained from Figure 9(b); [pct V]$_{equilibrium}$ is the equilibrium mass concentration of V; [pct C]$_L$ is the mass fraction of C in liquid phase under different super-gravity fields, and its value can be obtained from Figure 9(a); [pct C]$_{equilibrium}$ is the equilibrium mass concentration of C; $f_{S,VC}$ and f_{S,Mo_2C} are the formation solid fraction of VC and Mo_2C, respectively.

The variation of particle radius of VC and Mo_2C with solid fraction during solidification under different super-gravity coefficients is shown in Figure 11. According to the effect of super-gravity on the growth time of carbides, the growth time of VC is the earliest, and its solid fraction is not less than 0.8, which shows that the formation of carbides in super-gravity field is close to the solidification terminal. During solidification, the growth of primary carbides is limited by the element concentration of residual liquid phase. Because the formation of primary carbides needs to consume the elements contained in the carbides, this makes the size of primary carbides predicted in theory is larger than the actual size, but the theoretical calculation results can be used to explain the relation between the size of primary carbide and the super-gravity coefficient.

As shown in Figure 11, the particle sizes of VC and Mo_2C increase with the increase of solid fraction, but decrease with the increase of super-gravity coefficient. The reason is that the increase of the super-gravity coefficient is beneficial to reduce the degree of element segregation and element concentration in the liquid phase at the solidification front, resulting in the formation time of primary carbides closer to the end of solidification, thus reducing the growth time of primary carbides. In addition, a decrease in the liquid phase element concentration at the solidification front reduces the driving force of primary carbides growth.

C. *The Refinement Mechanism of Primary Carbides in Super-Gravity Fields*

The refinement mechanism of primary carbides in H13 steel solidified under super-gravity field is clarified in Figure 12. In Figures 12(c) through (e) and (h) through (k), the purple region represents dendrites, and the white region represents element segregation between dendrites. With the increase of the super-gravity coefficient, the degree of dendrite fragmentation is enhanced, which is easy to cause convective mass transfer of solute elements between dendrites. This weakens the degree of interdendritic element segregation, and delays the formation of

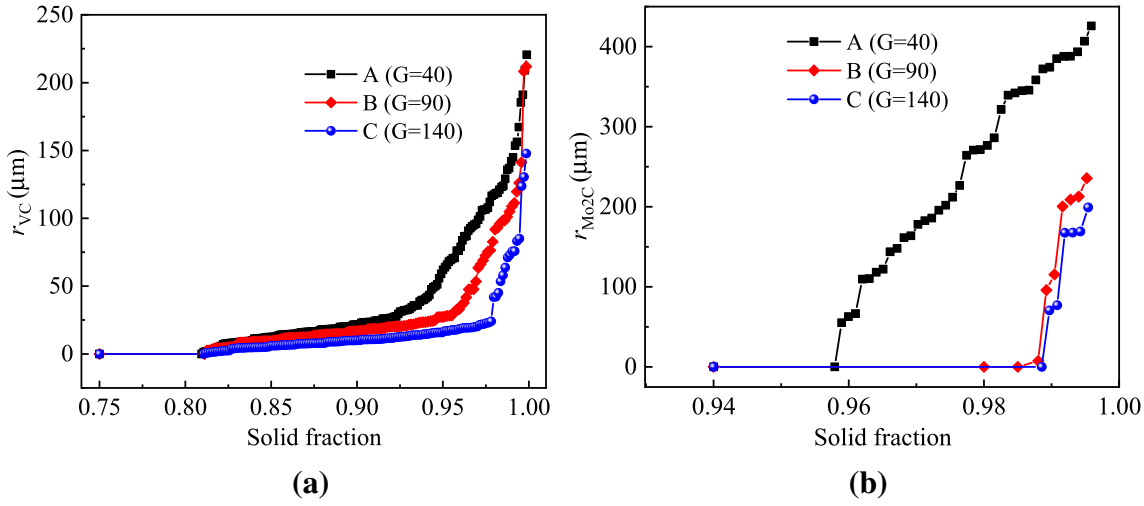

Fig. 11—The relationship between maximum generation radius of primary carbides with different types and solid fraction (*a*) VC, (*b*) Mo_2C.

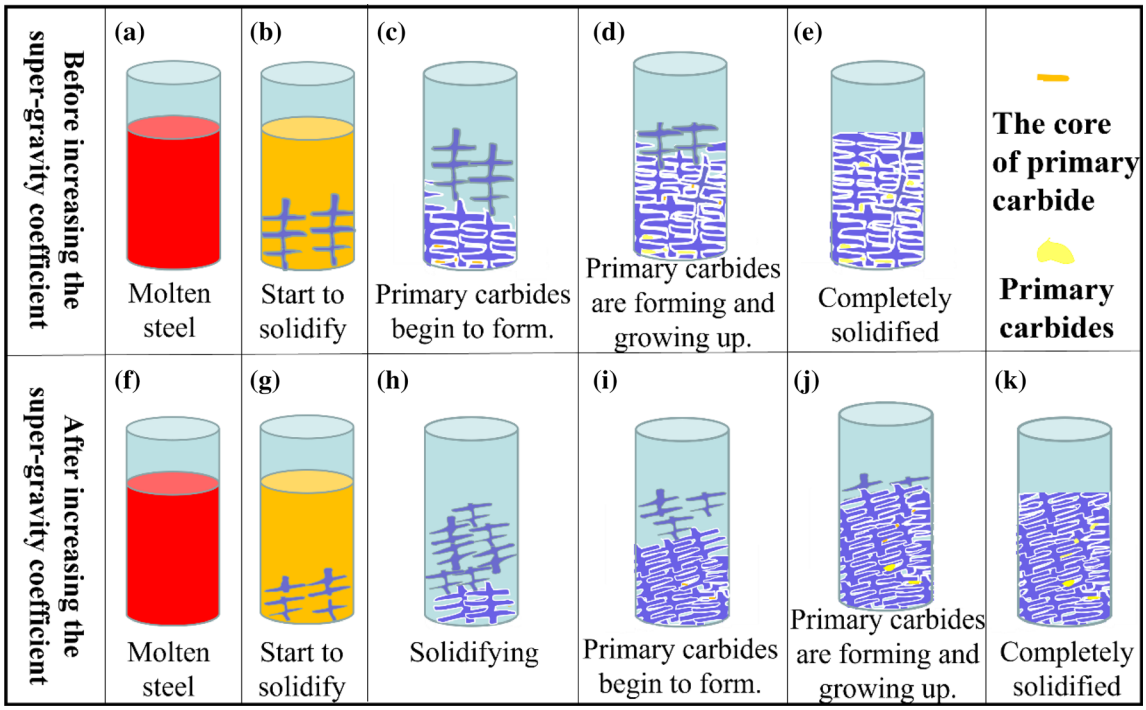

Fig. 12—Schematics of the refinement mechanism of primary carbides in casting solidified under super-gravity field (*a*) through (*e*) before increasing the super-gravity coefficient; (*f*) through (*k*) after increasing the super-gravity coefficient.

primary carbides. Therefore, the refinement of primary carbides in H13 steel was demonstrated to be effective under super-gravity field.

IV. CONCLUSIONS

In this work, the segregation of alloying elements and the characteristics of primary carbides in the super-gravity H13 steel castings were investigated, and the refinement mechanism of primary carbides was elucidated by thermodynamics and kinetics. The results obtained are as follows:

(1) With the increase of super-gravity coefficient, the number and size of V-rich and Mo-rich primary carbides decrease. When the super-gravity coefficient increases from 40 to 140, the total quantity and average area of the primary carbides decrease by 44 and 15.49 pct, respectively.
(2) The segregation ratio and width of the segregation zone of C, V, Cr, and Mo decrease with the increase of super-gravity coefficient. The segregation of Mo is the most serious, followed by V, Cr, and C. The segregation ratio of Mo is as high as 2.5, and the width of the segregation zone is about 25 μm.

(3) In super-gravity H13 castings, the primary carbides are produced in the solidification process with a solid fraction greater than 0.8. Compared with VC, the solid fraction at which Mo_2C begins to form is more easily affected by the super-gravity coefficient. As the super-gravity coefficient increases from 40 to 140, the solid fraction at which Mo_2C begins to form increases from 0.956 to 0.989.
(4) An increase in the super-gravity coefficient is conducive to reduce the maximum growth particle size of primary carbides. As the super-gravity coefficient increases from 40 to 140, the maximum generation radius of VC and Mo_2C decrease from 225 and 436 μm to 148 and 186 μm, respectively.

ACKNOWLEDGMENTS

This work was financially supported by China Postdoctoral Fund (Grant No. 2021M700394) and Key R&D Plan of Shandong Province in 2021 (Grant No. 2021CXGC010209). The authors thank the Beijing Key Laboratory of Special Melting and Preparation of High-end Metal Materials for its support.

CONFLICT OF INTEREST

On behalf of all authors, the corresponding author states that there is no conflict of interest.

REFERENCES

1. J. Zhu, Z.H. Zhang, and J.X. Xie: *Mater. Sci. Eng. A*, 2019, vol. 752, pp. 101–14.
2. C. Meng, H. Zhou, H.F. Zhang, X. Tong, D.L. Cong, C.W. Wang, and L.Q. Ren: *Mater. Des.*, 2013, vol. 51, pp. 886–93.
3. X.L. Sun, H.J. Guo, X.C. Chen, A.G. Ning, G.W. Du, and C.B. Shi: *Iron Steel*, 2014, vol. 49, pp. 68–73. (**In Chinese**).
4. K. Ozaki: *Denki Seiko*, 2005, vol. 76, pp. 249–57.
5. L.L. Mishnaevsky, N. Lippmann, and S. Schmauder: *Z. Metallkd.*, 2003, vol. 94, pp. 676–81.
6. J. Lan, J.J. He, W.J. Ding, Q.D. Wang, Y.P. Zhu, C.Q. Zhai, X.P. Xu, and C. Lu: *Iron Steel*, 2000, vol. 35, pp. 48–66. (**In Chinese**).
7. J. Lan, J.J. He, W.J. Ding, and Q.D. Wang: *ISIJ Int.*, 2000, vol. 40, pp. 1275–82.
8. Y. Huang, Y. Xie, G.G. Cheng, L. Chen, Y.D. Zhang, and Q.Z. Yan: *J. Chin. Soc. Rare Earths*, 2017, vol. 35, pp. 782–89. (**In Chinese**).
9. D. Wei: *Effect of Ce on Microstructure and Mechanical Properties of H13 Steel*, Inner Mongolia University of Technology, Huhehaote, 2015. (**In Chinese**).
10. Y.K. Pei, D.S. Ma, B.S. Liu, Z.Z. Chen, R. Zhou, and J. Zhou: *Iron Steel*, 2012, vol. 47, pp. 81–86. (**In Chinese**).
11. Z.Z. Chen and D. Lan: *Die Steel Manual*, Metallurgical Industry Press, Beijing, 2002. (**In Chinese**).
12. M.T. Mao, H.J. Guo, X.L. Sun, F. Wang, X.C. Chen, and J. Guo: *Chin. J. Eng.*, 2017, vol. 39, pp. 1174–81. (**In Chinese**).
13. S.N. Tewari: *Metall. Mater. Trans. A*, 1986, vol. 17A, pp. 2279–90.
14. B.S. Terry and O.S. Chinyamakobvu: *J. Mater. Sci.*, 1992, vol. 27, pp. 5666–70.
15. D.S. Ma, J. Zhou, Z.K. Zhang, H.X. Chi, and Z.Z. Chen: *Iron Steel*, 2010, vol. 45, pp. 80–84. (**In Chinese**).
16. M.T. Mao, H.J. Guo, F. Wang, and X.L. Sun: *ISIJ Int.*, 2019, vol. 59, pp. 848–57.
17. W.M. Mao, Z.S. Zhen, and H.T. Chen: *Spec. Cast. Nonferrous Alloys*, 2005, vol. 25, pp. 538–40. (**In Chinese**).
18. H. Zhang: Study on the fabrication and the solidification behavior of SiC_p/Al-Mg composites prepared by mechanical stirring [D]. Harbin: Harbin Institute of Technology, 2011. (**In Chinese**).
19. J. Yurko, R. Martinez, and M. Flemings: *Metall. Sci. Technol.*, 2003, vol. 21, pp. 10–15.
20. H.C. Zhu, H.B. Li, Z.Y. He, H. Feng, Z.H. Jiang, and T. He: *ISIJ Int.*, 2021, vol. 61, pp. 1889–98.
21. J. Li, Z.C. Guo, and J.T. Gao: *ISIJ Int.*, 2014, vol. 54, pp. 743–49.
22. X.C. Wen, L. Guo, Q.P. Bao, and Z.C. Guo: *J. Alloys Compd.*, 2020, vol. 832, pp. 154995–155007.
23. Y. Li, J.T. Gao, Z.L. Huang, and Z.C. Guo: *Ceram. Int.*, 2019, vol. 45, pp. 10961–68.
24. C. Li, J.T. Gao, Z. Wang, and H.R. Ren: *ISIJ Int.*, 2017, vol. 57, pp. 767–69.
25. Y. Lu, J.T. Gao, F. Wang, and Z.C. Guo: *Metall. Mater. Trans. B*, 2017, vol. 48B, pp. 749–53.
26. X. Lan, J.T. Gao, Z.L. Huang, and Z.C. Guo: *Metall. Mater. Trans. B*, 2018, vol. 49B, pp. 1165–73.
27. G.Y. Song, B. Song, Y.H. Yang, Z.B. Yang, and W.B. Xin: *Metall. Mater. Trans. B*, 2015, vol. 46, pp. 2190–97.
28. L. Guo, X.C. Wen, Q.P. Bao, and Z.C. Guo: *Metals*, 2018, vol. 8, pp. 701–13.
29. Y.H. Yang, B. Song, Z.B. Yang, G.Y. Song, Z.Y. Cai, and Z.C. Guo: *Materials*, 2016, vol. 9, pp. 1001–14.
30. L.X. Zhao, Z.C. Guo, Z. Wang, and M.Y. Wang: *Metall. Mater. Trans. A*, 2010, vol. 41A, pp. 670–75.
31. Y.N. Wang: *J. Iron Steel Res. Int.*, 2017, vol. 29, pp. 982–89.
32. J. Chen: *Data Manual of Common Charts in Steelmaking*, Metallurgical Industry Press, Beijing, 1984. (**In Chinese**).
33. M.T. Mao: *Study on Primary Carbides in H13 Steel and Its Control Method*, Beijing University of science and technology, Beijing, 2019. (**In Chinese**).